Published in final edited form as:

Prog Biophys Mol Biol. 2018 October ; 138: 105–115. doi:10.1016/j.pbiomolbio.2018.05.003.

Advanced Microscopy to Elucidate Cardiovascular Injury and Regeneration: 4D Light-Sheet Imaging

Kyung In Baek[1,*], **Yichen Ding**[1,2,*], **Chih-Chiang Chang**[1,*], **Megan Chang**[2], **René R. Sevag Packard**[2], **Jeffrey J. Hsu**[2], **Peng Fei**[3], and **Tzung K. Hsiai**[1,2,4]

[1]Department of Bioengineering, University of California, Los Angeles, Los Angeles, CA 90095

[2]Department of Medicine, David Geffen School of Medicine at University of California, Los Angeles, Los Angeles, CA 90095

[3]School of Optical and Electronic Information, Huazhong University of Science and Technology, Wuhan 430074, China

[4]Medical Engineering, California Institute of Technology, Pasadena, CA 91106

Abstract

The advent of 4-dimensional (4D) light-sheet fluorescence microscopy (LSFM) has provided an entry point for rapid image acquisition to uncover real-time cardiovascular structure and function with high axial resolution and minimal photo-bleaching/-toxicity. We hereby review the fundamental principles of our LSFM system to investigate cardiovascular morphogenesis and regeneration after injury. LSFM enables us to reveal the micro-circulation of blood cells in the zebrafish embryo and assess cardiac ventricular remodeling in response to chemotherapy-induced injury using an automated segmentation approach. Next, we review two distinct mechanisms underlying zebrafish vascular regeneration following tail amputation. We elucidate the role of

Corresponding Author: Tzung K. Hsiai, M.D., Ph.D., Department of Medicine (Cardiology) and Bioengineering, UCLA, 10833 Le Conte Ave., CHS17-054A, Los Angeles, CA 90095-1679, Thsiai@mednet.ucla.edu, Phone: 310-268-3839.

*These authors contributed equally to this work.

Author Disclosure Statement

The authors have no conflict of interest to disclose.

Credit Line

Reprinted with permission from ANTIOXIDANTS AND REDOX SIGNALING,

1. Flow-Responsive Vascular Endothelial Growth Factor Receptor-Protein Kinase C Isoform Epsilon Signaling Mediates Glycolytic Metabolites for Vascular Repair Volume 28, Issue 1, published by Mary Ann Liebert, Inc., New Rochelle, NY
2. Ultrafine Particle Exposure Reveals the importance of FOXO1/Notch Activation Complex for Vascular Regeneration. Volume 28, Issue 3, published by Mary Ann Lieber, Inc., New Rochelle, NY

Reprinted with permission from Scientific Reports,

1. Automated Segmentation of Light-Sheet Fluorescent Imaging to Characterize Experimental Doxorubicin-Induced Cardiac Injury and Repair, *Scientific Reports,* Article Number: 8603.
2. Cardiac Light-Sheet Fluorescent Microscopy for Multi-Scale and Rapid Imaging of Architecture and Function, *Scientific Reports*, Article Number: 22489

endothelial Notch signaling to restore vascular regeneration after exposure to the redox active ultrafine particles (UFP) in air pollutants. By manipulating the blood viscosity and subsequently, endothelial wall shear stress, we demonstrate the mechanism whereby hemodynamic shear forces impart both mechanical and metabolic effects to modulate vascular regeneration. Overall, the implementation of 4D LSFM allows for the elucidation of mechanisms governing cardiovascular injury and regeneration with high spatiotemporal resolution.

Keywords

Light-sheet fluorescence microscopy; cardiovascular injury; doxorubicin; vascular regeneration

Introduction

Zebrafish (*Danio rerio*) share conserved cardiovascular developmental signaling pathways with mammals, providing a genetically tractable model in developmental research, drug screening, and heart failure studies (Li et al., 2014; Packard et al., 2017; Power and Huisken, 2017; Tzahor and Poss, 2017; Vermot et al., 2009). Zebrafish embryos are optically transparent, allowing for real-time visualization of structural and functional phenotypes (Li et al., 2014; Opitz et al., 2012). Their small size and short developmental stages facilitate high-throughput genetic, epigenetic, and pharmaceutical analyses (Herzog et al., 2009; Sun et al., 2009). Although mammalian models including mice exhibit the capacity of tissue regeneration during the early stage of development, zebrafish demonstrate structural recovery in response to anatomical amputation, chemotherapy, or redox active ultrafine particles (UFP, diameter < 0.2 μm) in air pollutants (Li et al., 2014). In this review, we introduce our novel imaging technique using our custom-built light-sheet fluorescence microscopy (LSFM) to elucidate zebrafish models of cardiovascular injury and regeneration. We highlight the pathological effects of ambient UFP exposure underlying impaired Notch transcriptional activation complex to promote vascular regeneration (Baek et al., 2018b). Furthermore, we introduce a novel flow-responsive mechano-metabolic pathway implicated in vascular regeneration (Baek et al., 2018a).

1. Light-sheet imaging to study cardiovascular regeneration

Live imaging has transformed biomedical sciences by permitting visualization and analysis of dynamic cellular processes as they occur in their native contexts (Amos, 2000; Ntziachristos et al., 2005; Yuste, 2005). Conventional methods continue to be useful, but the pursuit of new biological insights often requires higher spatiotemporal resolution in ever-larger, intact samples and, crucially, a gentle touch, such that biological processes continue unhindered. Although confocal microscopy improves spatial resolution and image contrast, using the same path for both illumination and fluorescence detection leads to intensive photo-bleaching and photo-toxicity with limited penetration depth (100–150 μm) (Huisken et al., 2004; Keller and Stelzer, 2008). Multi-photon microscopy utilizes an infrared mode-locked laser as the illumination source and reaches up to 1 mm penetration depth (Horton et al., 2013; Kobat et al., 2011), but requires a high numerical aperture (NA > 0.7) and a short laser pulse with a long wavelength. On account of these limitations, LSFM splits the paths so that the illumination plane is perpendicular to the detection angle. Therefore, fluorescence

is emitted from the selective focal plane, and only a few fluorescent molecules are excited in the micrometer thickness of the light-sheet.

In comparison to conventional microscopy, LSFM integrates several distinct advantages (Chhetri et al., 2015; Mickoleit et al., 2014). (1) LSFM exposes the specimens to at least three orders of magnitude less light energy than confocal and multi-photon fluorescence microscopes over conventional excitation, thus greatly reducing photo-bleaching and photo-toxicity by two to five orders of magnitude (De Vos et al., 2014; Huisken and Stainier, 2009; Santi, 2011). In the absence of a pinhole, the loss of energy efficiency of the illumination beam is not more than 5% after transmission through the lenses and mirrors to scan a plane of sample. (2) LSFM allows for illuminating the desired sample area, significantly increasing signal efficiency and axial resolution. The thickness of the light-sheet generated by the illumination lens is the major determinant of the axial resolution whereas the axial resolution of other optical microscopes is predominately determined by the NA of the detection lens. (3) LSFM enables rapid imaging at 100 frames/sec (~400 megapixels/sec) after applying a sCMOS or CCD camera with a large dynamic range, far more than the 10 megapixels/sec of confocal or multi-photon microscopy. (4) LSFM also provides higher signal-to-noise ratio which is over 100:1, while that of confocal microscopy is 60:1 and multi-photon microscopy is only 10:1. LSFM for the present experimental data set was carried out on previously developed systems (Fig. 1A) (Ding et al., 2017a; Ding et al., 2017b; Fei et al., 2016; Lee et al., 2016; Packard et al., 2017; Sideris et al., 2016; Sung et al., 2016). The detection path, including an objective lens (10x/0.25, Nikon), a tube lens (ITL 200, Thorlabs), and switchable optical filters (Semrock, NewYork, USA), was placed orthogonal to the illumination plane for collecting fluorescence signals (Fig. $1B_{1–2}$). Digital images were recorded with a high frame rate by using two scientific CMOS cameras (ORCA-Flash4.0 V2, Hamamatsu, Japan) for dual-channel detection (Fig. $1B_3$). A diode-pumped solid-state laser containing four wavelengths of 405 nm, 473 nm, 532 nm, and 589 nm (Laserglow Technologies, Toronto, Canada) was used as the illumination source (Fig. $1B_4$). Three common light-sheet configurations were generated to illuminate the embryonic zebrafish heart (150–250 μm), adult zebrafish heart (500–1500 μm), and neonatal mouse heart (3000–5000 μm) (Fig.$1C_1$). The confocal region of the light-sheet was used as a uniform planar illumination and was finely stretched to cover the sample's transverse dimension (Fig.$1C_2$). The extent of axial projection was directly imaged at the waist of the light-sheet by the profiler, and the confocal range was further reconstructed by stacking the projections (Fig. $1C_2$). The thickness of the light-sheet, defined as the axial full width at half maximum (FWHM) value of the beam waist, was measured at ~5 μm for the embryonic zebrafish heart (i), ~9 μm for the adult zebrafish heart (ii), and ~18 μm for the neonatal mouse heart (iii) (Fig. $1C_{1–2}$). The lateral confocal regions with respect to these three axial extents were profiled (Fig. 1C2 i–iii). The detection objectives were 10x/0.3 (Plan Fluor, Nikon, Japan) for the embryonic zebrafish heart, 4x/0.13 (Plan Fluor, Nikon, Japan) for the adult zebrafish heart, and 1x/0.25 (MVX10, Olympus, Japan) for the neonatal mouse heart to capture the full region-of-interest (ROI). Once the thickness of the light-sheet for excitation and the objective lens for detection were determined, the lateral and axial resolution for each configuration could be obtained by measuring the point spread function (PSF). The fluorescent point source (polystyrene beads) was imaged by applying the

aforementioned three light-sheet configurations and demonstrated the lateral and axial resolution by measuring the FWHMs from x-y, x-z, and y-z plane images (Fig. $1C_3$).

LSFM has the capacity to localize the 4D cellular phenomena with multi-fluorescence channels to study cardiovascular development and regeneration. Unlike commercial systems, including the ASI iSPIM, Zeiss Z.1, Leica SP8 and LaVision Ultramicroscope. Our multi-scale LSFM strategy is capable of rapid imaging acquisition to elucidate mechanisms of vascular regeneration after injury in the zebrafish cardiovascular system. In comparison with the ASI iSPIM, Zeiss Z.1 and Leica SP8 (Keller et al., 2008; Kumar et al., 2014; Wu et al., 2011; Wu et al., 2013), we applied dry objective lenses with long-working distances to provide a large field-of-view. We further implemented a cylindrical lens to reshape the Gaussian beam to achieve high spatiotemporal resolution without the need for laser scanning the contracting heart (Lee et al., 2016; Power and Huisken, 2017). In addition, our system minimizes photo-bleaching and photo-toxicity due to the planar illumination (Power and Huisken, 2017). In contrast to the LaVision Ultramicrope optimized for mouse brain (Dodt et al., 2007), our LSFM system enables live imaging of zebrafish embryos. Furthermore, our custom-built system adapts a retrospective synchronization algorithm to reconstruct contracting embryonic hearts in 4D (Lee et al., 2016). We have also demonstrated a resolution-enhancement method for using the objective lenses with low NA objectives, allowing for multi-scale imaging with a large field-of-view (Fei et al., 2018). For these reasons, our custom-built LSFM has the capacity to perform the image-guided study for cardiovascular regeneration.

However, the main limitation of LSFM reside in photon scattering or absorption in the setting of imaging acquisition of large specimens (such as the rodent heart) or interfacing with mismatching refractive indices (from inadequate tissue clearing). Other limitations include the effect of out-of-focus light to reduce the signal-to-noise ratio. As a result of absorption, refraction, and scattering of coherent light within the tissue, these limitations generate stripe or shadow artifacts to attenuate the image. The lateral resolution of LSFM is lower than that of confocal imaging by the factor of $\sqrt{2}$ when the same objectives are used (Cannell et al., 2006). The advantages and disadvantages among the different optical modalities are summarized in Table 1.

1.1. Light-sheet imaging with automated segmentation method to analyze doxorubicin-induced cardiac injury and regeneration—

In adult zebrafish, regenerating myocardium electrically couples with uninjured myocardium (Lee et al., 2014), providing a conserved cardiomyopathy model (Ding et al., 2011). Precise assessment of cardiac ventricular architecture remains an imaging challenge due to the small size of the heart. The advent of the chemical clearing method enabled multi-scale imaging of hearts from zebrafish embryos (hundreds of μm in diameter) to adult fish (1–2 mm in diameter) (Fei et al., 2016; Sung et al., 2016). In the setting of a simplified tissue clearing method using benzyl alcohol-benzyl benzoate (BABB) to improve laser penetration and to achieve optical transparency, we visualized volumetric changes of cardiac morphology in adult zebrafish in response to doxorubicin-induced cardiac toxicity by combining light-sheet illumination with a customized automated segmentation method based on histogram analysis (Fig. 2A). Doxorubicin is an anthracycline agent that is commonly used in chemotherapy

regimens for patients with a variety of cancers, and it is well known to cause cardiac injury, often limiting its use clinically (Volkova and Russell, 2011). The transgenic *Tg(cmlc2:GFP)* zebrafish line was used to visualize ventricular remodeling after doxorubicin chemotherapy. The detection objective is imaged through the liquid-air interface where it is introduced to a spherical aberration-based PSF extension (Tomer et al., 2015). The section thickness (1–5 μm) of mechanical scanning was determined based on the Nyquist-Shannon sampling theorem, while image acquisition was done with an exposure time of between 10–50 ms. Thus, the spatial resolution of the LSFM in cross-section varied from 1 μm to 10 μm, while the waist ω_0 ranged from 2 to 9 μm. Reconstructed image stacks underwent alpine interpolation and iterative 3D deconvolution to compensate under-sampling of the camera and to prevent blurred images. A 4-step automated image segmentation process was then applied to the input images for precise assessment of the structural reorganization of the adult zebrafish heart, as previously described (Packard et al., 2017). Cardiac volumes assessed with automated segmentation were quantitatively compared following 3, 30, and 60 days of doxorubicin treatment (Fig. 2B). Our present data revealed 3 days of doxorubicin treatment led to global cardiac injury and resulted in the reduction of both endocardial and myocardial volumes, followed by ventricular remodeling at day 30, and complete regeneration and restoration of normal architecture at day 60. Furthermore, the automated segmentation method established a well-defined structure of the atrium, ventricle, and bulbus arteriosus, revealing ventricular trabeculae and ultrastructure (Fig. 3A–B, D). The computation of the angle between the atrio-ventricular (AV) valves and ventricular-bulbar (VB) valves permitted precise assessment, including the ventricular inflow (dotted yellow line) and outflow path (solid yellow line) (Fig. 3C). Our results accentuate the suitability of light-sheet imaging combined with automated segmentation as a high-throughput method to monitor 3D cardiac ultrastructural changes in adult zebrafish, with translational implications to drug discovery and modifiers of chemotherapy-induced cardiomyopathy.

1.2. LSFM to study mechano-transduction and vascular dynamics—With the use of the transgenic *Tg*(*flk1:GFP; Gata1:Ds-red*) zebrafish line which drives of the expressions of VEGFR2 as well as erythrocytes, we simultaneously detected circulating erythrocytes and demonstrated flow-mediated vascular regeneration. Our previous study established a zebrafish tail amputation model to seek mechanisms underlying vascular regeneration after injury (Baek et al., 2018a). The posterior tail segments of the embryos were amputated with a sterilized surgical scalpel under a stereomicroscope and immobilized with low melting agarose in a fluorinated ethylene propylene tube to achieve a uniform refractive index for fluorescence detection. Imaging cellular dynamics across large specimens requires high spatiotemporal resolution, uniform light-sheet thickness and low photo-bleaching/-toxicity. LSFM enables image acquisition of dynamic biophysical and biochemical activities such as blood flow or a beating heart at > 100 frames/sec. The precise alignment of dual-channel detection of LSFM further allows us to concurrently acquire the structure of the vasculature and circulating erythrocytes to perform 2D particle imaging velocimetry (PIV) in the dorsal aorta (DA) (Fig. 4A–E). The tail amputation model with LSFM offers a flexible platform to study hemodynamic regulation on endothelial vascular regeneration (Fig. 4F–G), providing an entry point to study mechano-transduction in a low Reynolds number system (Re: 100 ~ 1000). Besides, LSFM imaging has also been implemented in various developmental

studies, such as 4D reconstruction of contracting zebrafish hearts (Lee et al., 2016; Mickoleit et al., 2014), time-lapse imaging of neural activity and cell lineages in *Drosophila* (Ahrens et al., 2013; Keller et al., 2010; Tomer et al., 2012; Truong et al., 2011; Vladimirov et al., 2014), *C. elegans* (Wu et al., 2011), zebrafish (Bassi et al., 2015; Chhetri et al., 2015; Forouhar et al., 2006; Lenard et al., 2015; Schmid et al., 2013; Weber et al., 2017; Wu et al., 2013) and mice (Bouchard et al., 2015). Unique characteristics of LSFM permit long-term imaging of cardiovascular regeneration and development. In comparison to the aforementioned studies, visualization of the periodic contractions of the embryonic heart requires either a 4D synchronization algorithm (Ding et al., 2017a; Liebling et al., 2005; Mickoleit et al., 2014) or a volumetric imaging method, while capturing dynamic blood flow in 4D is still underway.

2. Zebrafish tail amputation model to study vascular regeneration after injury 2.1. Exposure to ambient UFP reveals importance of Notch signaling for vascular regeneration

Ambient particulate matter ($PM_{2.5}$) in air pollutants is an emerging epigenetic factor in promoting endothelial dysfunction (Karimi Galougahi et al., 2016; Minicucci et al., 2009). Recent epidemiological studies have consistently supported that $PM_{2.5}$ exposure results in elevated risk of cancer, respiratory diseases, and cardiovascular defects during development (Brook et al., 2010; Brunekreef and Holgate, 2002; Dadvand et al., 2011; Gorham et al., 1989; Hwang et al., 2015; Ritz et al., 2002). UFP are a major sub-fraction of $PM_{2.5}$ and comprise a mixture of highly reactive organic chemicals (Sardar et al., 2005) and transition metals (Brook et al., 2010; Lough et al., 2005; Nel et al., 2006; Zhang et al., 2008). Exposure to UFP promotes Jun amino-terminal kinase (JNK) expression to produce a reactive oxygen species (ROS), thereby increasing vascular oxidative stress, and is also implicated in NF-κB-mediated inflammatory responses that induce atherosclerosis and vascular calcification (Araujo et al., 2008; Brook et al., 2010; Li et al., 2013; Li et al., 2009; Nel et al., 2006; Pope et al., 2004; Zhang et al., 2008).

The Notch signaling pathway is an evolutionarily conserved intracellular signaling pathway intimately involved in cell-fate determination (Bray, 2016; MacKenzie et al., 2004; Quillard et al., 2008; Rostama et al., 2014; Walshe et al., 2011) and regulates initial sprout formation during angiogenesis (Baonza and Garcia-Bellido, 2000; Fre et al., 2005; Hellstrom et al., 2007; Jensen et al., 2000; Krebs et al., 2000; Lobov et al., 2007; Pellegrinet et al., 2011; Stanger et al., 2005). Upon ligand binding, Notch receptors undergo proteolytic cleavages to release the Notch Intracellular Cytoplasmic Domain (NICD) under regulation of a disintegrin and metalloproteinases (ADAM) family. Following translocation to the nucleus, NICD forms a transcriptional activation complex to induce downstream Notch target genes, including Hairy and enhancer of split-1 (*Hes1*) and *gridlock* (Bray, 2016). Ablation of Notch1 is associated with developmental retardation resulting in embryonic lethality, whereas dysregulated Notch1 activity in endothelial cells induces aberrant proliferation, resulting in a hyperplastic vascular network (Artavanis-Tsakonas et al., 1999). Missense mutation of the Notch3 gene underlies the development of the degenerative vascular disease known as Cerebral Autosomal-Dominant Arteriopathy with Subcortical Infarcts and Leukoencephalopathy (CADASIL) (Joutel et al., 1996).

To investigate whether UFP mitigate Notch-mediated vascular regeneration, we crossbred the Notch reporter transgenic fish *Tg(tp1:GFP)* with the *Tg(flk1:mCherry)* line to image Notch activity-mediated vascular regeneration. The Epstein-Barr Virus terminal protein 1 (tp1) reporter contains two Notch-responsive elements on the Rbp-Jκ binding sites for NICD, thereby reporting regional Notch1b activation (Lee et al., 2016). The control group developed vascular regeneration and formed a loop between the DA and the dorsal longitudinal anastomotic vessel (DLAV) with prominent endothelial Notch activity (as visualized in yellow) on the site of injury at 3 days post amputation (dpa). On the other hand, UFP exposure resulted in significant reduction of vascular endothelial Notch activity followed by disrupted vascular network formation on the injured site. The ADAM10 inhibitor, GI254023X, which inhibits proteolytic activation of the Notch receptor, recapitulated Notch-mediated impaired vascular regeneration. To further investigate whether the reduction of Notch signaling is associated with vascular impairment after the injury, we constructed dominant-negative *Notch1b* (DN-*Notch1b*) mRNA that attenuated Notch signaling by 96%. Approximately 75% of Notch-knockdown embryos underwent aberrant vascular regeneration and network formation, exhibiting embryonic lethality at 5 dpa. *NICD* mRNA micro-injection as a means to up-regulate Notch signaling restored UFP-, ADAM10 inhibitor-, and DN-*Notch1b* mRNA- attenuated Notch activity and consequent vascular regeneration. By using our well-established zebrafish tail amputation model, we provide a molecular basis to assess the effects of UFP on endothelial function for vascular regeneration (Fig. 5).

Epidemiological studies consistently support a link between maternal exposure to air pollutants and increased risk of congenital cardiovascular diseases (Dadvand et al., 2011). UFP in air pollutants are the products of incomplete combustion from urban environmental sources, including diesel trucks and gasoline vehicles, and are enriched by elemental and polycyclic aromatic hydrocarbons (Chhetri et al., 2015). Their large surface-to-volume ratio increases potential absorption to the pulmonary and cardiovascular systems (Frampton, 2001; Nemmar et al., 2002; Schulz et al., 2005). UFP exposure via inhalation facilitates plasma lipid metabolite production and increases high-density lipoprotein oxidant capacity to accelerate atherosclerosis in LDLR-null mice (Li et al., 2013). UFP exposure further regulates atherogenic lipid metabolites and promotes macrophage infiltration in the intestine (Chhetri et al., 2015), where the composition of the micro-biota is altered to elevate atherogenic lipid metabolite levels. The emerging role of redox-sensitive micro-RNAs (miRs) have been implicated in cellular proliferation (Wu et al., 2012; Yu et al., 2012). $PM_{2.5}$ have been reported to modulate the levels of a number of miRNAs, including miR-223 and miR-375 (Bleck et al., 2013; Rodosthenous et al., 2016; Yang et al., 2017). Therefore, UFP could regulate the level of miRs for Notch inhibition (Li et al., 2017).

Nevertheless, the mechanism underlying endothelial proliferation and vascular regeneration remains elusive due to the demand of high spatial and temporal resolution of real-time 3-D imaging. Scanning methods such as confocal or multi-photon microscopy are able to provide sufficient lateral resolution to reveal the biophysical dynamics at the cellular level, but are confined to sequential raster scanning over the specimen. For instance, confocal microscopy allows for capturing angiogenic sprouts at a particular time but is limited in time-lapse imaging due to rapid photo-bleaching (Gerhardt et al., 2003; Hogan et al., 2009; Nguyen et

al., 2013). However, selective-plane illumination and concurrent detection in a 2D plane enable to implement time-lapse visualization of regenerating endothelial vasculature with the minimal photo-bleaching and photo-toxicity. The signal-to-noise ratio and axial resolution of LSFM are also improved due to planar illumination; otherwise, the focus of detection gradually degrades in the deep tissue. Therefore, the shorter exposure time, the deeper penetration depth, and the higher spatiotemporal resolution allow for time-lapse imaging of vascular regeneration and cellular dynamics in live zebrafish embryos, and LSFM provides the basis for revealing the mechanisms underlying cardiovascular regeneration and development.

2.2. Shear stress modulation of vascular dynamics and regeneration— Hemodynamic blood flow exerts shear stress, cyclic stretch, and hydrostatic pressure on the endothelium (Ando and Yamamoto, 2011; Li et al., 2005). While cyclic stretch plays an important role in maintaining endothelial function, it is well recognized that hemodynamic shear forces mechanically and metabolically modulate vascular endothelial function (Cheng et al., 2007; Lee et al., 2015; Li et al., 2015). A complex flow profile develops at the arterial bifurcations, where flow separation and migrating stagnation points create disturbed flow (DF), mediating the focal and eccentric nature of atherosclerotic lesions (Chiu et al., 1998; Dewey Jr et al., 1981; Ding et al., 2013; Frangos et al., 1996; Hwang et al., 2003a; Hwang et al., 2003b; Surapisitchat et al., 2001). A recent study examined the role of laminar shear stress in driving expression of vascular endothelial growth factor (VEGF) and endothelial nitric oxide synthase (eNOS)-mediated Protein Kinase C isoform epsilon (PKCε) to modulate endothelial cell (EC) proliferation and lumen formation (Koh et al., 2009; Rask-Madsen and King, 2008). Unidirectional pulsatile (PSS) and oscillatory shear stress (OSS) differentially modulate the canonical Wnt/β-catenin pathway to modulate vascular development and regeneration (Dejana, 2010; Li et al., 2014), while also being implicated in the differentiation of vascular progenitors during angiogenesis (Boselli et al., 2015; Roman and Pekkan, 2012).

Endothelial glycolysis is mechano-responsive (Suarez and Rubio, 1991), and ECs are highly glycolytic (De Bock et al., 2013a). ECs further increase the level of glycolytic flux when switching from quiescence to a proliferative state, while the glycolytic enzyme, 6-phosphofructo-2-kinase/fructose-2,6-biphosphatase 3 (PFKFB3), localizes in lamellipodia (De Bock et al., 2013b). As a critical regulator of glycolysis, PFKFB3 further involves lamellipodia/filopodia extension during vessel formation (De Bock et al., 2013a; De Bock et al., 2013b). Laminar shear stress modulates the expression of Krüppel-like factor 2 (KLF2) to suppress PFKFB3-mediated endothelial glycolysis and vessel sprouting (Doddaballapur et al., 2015), whereas disturbed flow mitigates mitochondrial respiration and increases basal glycolysis and glycolytic capacity (Wu et al., 2017).

Our recent study with zebrafish supports the notion that PSS and OSS differentially modulate VEGFR-PKCε signaling to induce PFKFB3-mediated glycolytic metabolites for vascular repair (Baek et al., 2018a). Use of embryonic zebrafish allowed for genetic manipulation of blood viscosity to alter the level of endothelial wall shear stress (Galloway et al., 2005) to modulate the PKCε-PFKFB3 pathway *in vivo* (Fig. 6A). *Gata1a* morpholino oligonucleotide (MO) micro-injection prevented erythrocyte production, thereby reducing

the level of viscosity-mediated shear stress compared to control (Fig. 6Ai–ii). (Kulkeaw and Sugiyama, 2012; Vermot et al., 2009). On the other hand, *EPO* mRNA micro-injection resulted in elevated erythrocytosis as a means of augmenting viscosity-mediated wall shear stress (Fig. 6Aiii) (Chu et al., 2007). In the transgenic *Tg(flk1:GFP)* zebrafish model of tail regeneration, control *p53* MO injection demonstrated vascular regeneration, as visualized by a closed loop between the DA and the DLAV at 3 dpa. In contrast, suppressing the level of PKCε with MO injection developed aberrant vascular regeneration. Furthermore, micro-injection of *Gata1a* MO delayed vascular regeneration from 3 dpa to 5 dpa. The micro-injection of cardiac troponin T2 (*Tnnt2*) MO to arrest myocardial contraction and subsequent blood flow further attenuated vascular regeneration at 3 dpa, while embryos failed to thrive at 5 dpa. On the other hand, erythropoietin (*EPO*) mRNA micro-injection promoted tail regeneration. As a corollary, *PKCε* mRNA restored vascular regeneration in *Gata1a* MO injected embryos at 3 and 5 dpa (Fig. 6B).

In reference to our metabolomic analysis via gas chromatography time-of-flight mass spectrometry (GC-TOF), we elucidated that shear stress regulates glycolytic metabolites, including glucose ($C_6H_{12}O_6$), fructose ($C_6H_{12}O_6$), and dihydroxyacetone ($C_3H_6O_3$, DHA) via PFKFB3. In the zebrafish tail amputation model, exposure to DHA increased the proportion of zebrafish embryos with complete regeneration in the control group, whereas it rescued vascular repair in the absence of PKCε (Fig. 7). Our findings support that flow-responsive PKCε modulates endothelial glycolytic metabolites that are implicated in vascular regeneration. The advent of high-throughput “omics” approaches, including epigenomics, transcriptomics, miRnomics, proteomics, and metabolomics (Simmons et al., 2016), has provided new mechanotransduction strategies to discover biomarkers with therapeutic targets.

Current scanning methods are limited by their sequential point-scanning strategy in 2D planes, being insufficient to elucidate hemodynamic shear forces during cardiac morphogenesis. Unlike conventional bright-field microscopy, LSFM applies orthogonal illumination and detection, enabling investigators to selectively localize mechano-transduction to the endocardial endothelial lining within an ultra-thin plane of the sample. Due to the rapid multi-channel detection at the single cellular level, LSFM allows for the simultaneous imaging of the blood flow at the injured site and 3D structure of the vessels, elucidating hemodynamics with underlying the initiation of endocardial trabeculation during cardiac development (Lee et al., 2016). In conclusion, LSFM allows for rapid tracking of fluorescently labeled targets in multiple channels, thereby providing a computational basis to quantify blood flow and hemodynamic shear forces.

Conclusion and Outlook

Zebrafish have been utilized as an emerging developmental model due to a conserved physiology and anatomy with mammals. Its optical transparency at the embryonic stage facilitates direct observation of organogenesis including cardiovascular morphogenesis. While zebrafish comprise a well-established genetic system for studying cardiovascular development and disease, zebrafish demonstrate unique regenerative capacity in response to anatomical or chemotherapy-induced injury. Both high spatiotemporal resolution and deep

tissue penetration are required to tracking cardiovascular dynamics, such as the regenerating ventricular ultrastructure. Therefore, LSFM is suitable to monitor spatiotemporal variations of the regenerating cardiovascular system with minimal photo-bleaching /-toxicity, and is also a promising approach to track single blood cells as well as estimating the parabolic velocity distribution of blood flow in the embryonic zebrafish model. In addition, parallel advances in deep learning and virtual reality may lead us to more precisely elucidating cardiovascular architecture and function in future studies. Developing a novel convolutional or recurrent neural network for automatic segmentation will benefit image post-processing procedures that are otherwise limited in accuracy and efficiency by manual segmentation in the setting of large data sets (Lawrence et al., 1997; Shelhamer et al., 2017; Zheng et al., 2015). The study of interactive virtual reality establishes an efficient and robust framework for creating a user-directed microenvironment in which we are able to unravel developmental cardiac mechanics and physiology with high spatiotemporal resolution (Ding et al., 2017a; Eliceiri et al., 2012; Peng et al., 2010; Peng et al., 2014). In this review, we address our zebrafish model of injury with a mechanistic approach to understand cardiovascular regeneration. Furthermore, our findings with zebrafish combined with multi-scale light-sheet imaging demonstrate the advantages of light-sheet imaging, highlighting its role as a novel imaging strategy that can illuminate the mechanisms of cardiovascular injury and repair and further advance the field.

Acknowledgments

This study was supported by the National Institutes of Health HL118650 (T.K.H.), HL083015 (T.K.H.), HL111437 (T.K.H.), HL129727 (T.K.H.), T32 training grant HL007895 (J.J.H.), and an AHA Scientist Development Grant 16SDG30910007 (R.R.S.P).

References

1. Ahrens MB, Orger MB, Robson DN, Li JM, Keller PJ. Whole-brain functional imaging at cellular resolution using light-sheet microscopy. Nat Methods. 2013; 10:413–20. [PubMed: 23524393]
2. Amos B. Lessons from the history of light microscopy. Nat Cell Biol. 2000; 2:E151–2. [PubMed: 10934490]
3. Ando J, Yamamoto K. Effects of shear stress and stretch on endothelial function. Antioxid Redox Signal. 2011; 15:1389–403. [PubMed: 20854012]
4. Araujo JA, Barajas B, Kleinman M, Wang X, Bennett BJ, Gong KW, Navab M, Harkema J, Sioutas C, Lusis AJ, Nel AE. Ambient particulate pollutants in the ultrafine range promote early atherosclerosis and systemic oxidative stress. Circ Res. 2008; 102:589–96. [PubMed: 18202315]
5. Artavanis-Tsakonas S, Rand MD, Lake RJ. Notch signaling: cell fate control and signal integration in development. Science. 1999; 284:770–6. [PubMed: 10221902]
6. Baek KI, Li R, Jen N, Choi H, Kaboodrangi A, Ping P, Liem D, Beebe T, Hsiai TK. Flow-Responsive Vascular Endothelial Growth Factor Receptor-Protein Kinase C Isoform Epsilon Signaling Mediates Glycolytic Metabolites for Vascular Repair. Antioxid Redox Signal. 2018a; 28:31–43. [PubMed: 28762754]
7. Baek KI, Packard RRS, Hsu JJ, Saffari A, Ma Z, Luu AP, Pietersen A, Yen H, Ren B, Ding Y. Ultrafine Particle Exposure Reveals the Importance of FOXO1/Notch Activation Complex for Vascular Regeneration. Antioxidants & redox signaling. 2018b; 28:1209–1223. [PubMed: 29037123]
8. Baonza A, Garcia-Bellido A. Notch signaling directly controls cell proliferation in the Drosophila wing disc. Proc Natl Acad Sci U S A. 2000; 97:2609–14. [PubMed: 10706613]

9. Bassi A, Schmid B, Huisken J. Optical tomography complements light sheet microscopy for in toto imaging of zebrafish development. Development. 2015; 142:1016–20. [PubMed: 25655702]
10. Bleck B, Grunig G, Chiu A, Liu M, Gordon T, Kazeros A, Reibman J. MicroRNA-375 regulation of thymic stromal lymphopoietin by diesel exhaust particles and ambient particulate matter in human bronchial epithelial cells. J Immunol. 2013; 190:3757–63. [PubMed: 23455502]
11. Boselli F, Freund JB, Vermot J. Blood flow mechanics in cardiovascular development. Cell Mol Life Sci. 2015; 72:2545–59. [PubMed: 25801176]
12. Bouchard MB, Voleti V, Mendes CS, Lacefield C, Grueber WB, Mann RS, Bruno RM, Hillman EM. Swept confocally-aligned planar excitation (SCAPE) microscopy for high-speed volumetric imaging of behaving organisms. Nature photonics. 2015; 9:113. [PubMed: 25663846]
13. Bray SJ. Notch signalling in context. Nat Rev Mol Cell Biol. 2016; 17:722–735. [PubMed: 27507209]
14. Brook RD, Rajagopalan S, Pope CA 3rd, Brook JR, Bhatnagar A, Diez-Roux AV, Holguin F, Hong Y, Luepker RV, Mittleman MA, Peters A, Siscovick D, Smith SC Jr, Whitsel L, Kaufman JD. American Heart Association Council on E, Prevention CotKiCD, Council on Nutrition PA and Metabolism. Particulate matter air pollution and cardiovascular disease: An update to the scientific statement from the American Heart Association. Circulation. 2010; 121:2331–78. [PubMed: 20458016]
15. Brunekreef B, Holgate ST. Air pollution and health. Lancet. 2002; 360:1233–42. [PubMed: 12401268]
16. Cannell M, McMorland A, Soeller C, Pawley J. Book Handbook of biological confocal microscopy. New York, NY: Springer, City; 2006. Handbook of biological confocal microscopy.
17. Cheng C, Tempel D, van Haperen R, de Boer HC, Segers D, Huisman M, van Zonneveld AJ, Leenen PJ, van der Steen A, Serruys PW, de Crom R, Krams R. Shear stress-induced changes in atherosclerotic plaque composition are modulated by chemokines. J Clin Invest. 2007; 117:616–26. [PubMed: 17304353]
18. Chhetri RK, Amat F, Wan Y, Höckendorf B, Lemon WC, Keller PJ. Whole-animal functional and developmental imaging with isotropic spatial resolution. Nature methods. 2015; 12:1171. [PubMed: 26501515]
19. Chiu JJ, Wang DL, Chien S, Skalak J, Usami S. Effects of disturbed flow on endothelial cells. Journal of biomechanical engineering. 1998; 120:2–8. [PubMed: 9675673]
20. Chu C-Y, Cheng C-H, Chen G-D, Chen Y-C, Hung C-C, Huang K-Y, Huang C-J. The zebrafish erythropoietin: functional identification and biochemical characterization. FEBS letters. 2007; 581:4265–4271. [PubMed: 17706649]
21. Dadvand P, Rankin J, Rushton S, Pless-Mulloli T. Ambient air pollution and congenital heart disease: a register-based study. Environ Res. 2011; 111:435–41. [PubMed: 21329916]
22. De Bock K, Georgiadou M, Carmeliet P. Role of endothelial cell metabolism in vessel sprouting. Cell Metab. 2013a; 18:634–47. [PubMed: 23973331]
23. De Bock K, Georgiadou M, Schoors S, Kuchnio A, Wong BW, Cantelmo AR, Quaegebeur A, Ghesquiere B, Cauwenberghs S, Eelen G, Phng LK, Betz I, Tembuyser B, Brepoels K, Welti J, Geudens I, Segura I, Cruys B, Bifari F, Decimo I, Blanco R, Wyns S, Vangindertael J, Rocha S, Collins RT, Munck S, Daelemans D, Imamura H, Devlieger R, Rider M, Van Veldhoven PP, Schuit F, Bartrons R, Hofkens J, Fraisl P, Telang S, Deberardinis RJ, Schoonjans L, Vinckier S, Chesney J, Gerhardt H, Dewerchin M, Carmeliet P. Role of PFKFB3-driven glycolysis in vessel sprouting. Cell. 2013b; 154:651–63. [PubMed: 23911327]
24. De Vos WH, Beghuin D, Schwarz CJ, Jones DB, van Loon JJ, Bereiter-Hahn J, Stelzer EH. Invited Review Article: Advanced light microscopy for biological space research. Rev Sci Instr. 2014; 85:101101.
25. Dejana E. The role of wnt signaling in physiological and pathological angiogenesis. Circ Res. 2010; 107:943–52. [PubMed: 20947863]
26. Dewey CF Jr, Bussolari SR, Gimbrone MA Jr, Davies PF. The dynamic response of vascular endothelial cells to fluid shear stress. Journal of biomechanical engineering. 1981; 103:177–185. [PubMed: 7278196]

27. Ding Y, Abiri A, Abiri P, Li S, Chang C-C, Baek KI, Hsu JJ, Sideris E, Li Y, Lee J. Integrating light-sheet imaging with virtual reality to recapitulate developmental cardiac mechanics. JCI insight. 2017a:2.

28. Ding Y, Lee J, Ma J, Sung K, Yokota T, Singh N, Dooraghi M, Abiri P, Wang Y, Kulkarni RP. Light-sheet fluorescence imaging to localize cardiac lineage and protein distribution. Sci Rep. 2017b; 7:42209. [PubMed: 28165052]

29. Ding Y, Sun X, Huang W, Hoage T, Redfield M, Kushwaha S, Sivasubbu S, Lin X, Ekker S, Xu X. Haploinsufficiency of Target of Rapamycin Attenuates Cardiomyopathies in Adult ZebrafishNovelty and Significance. Circ Res. 2011; 109:658–669. [PubMed: 21757652]

30. Ding Z, Liu S, Wang X, Khaidakov M, Dai Y, Mehta JL. Oxidant stress in mitochondrial DNA damage, autophagy and inflammation in atherosclerosis. Sci Rep. 2013; 3:1077. [PubMed: 23326634]

31. Doddaballapur A, Michalik KM, Manavski Y, Lucas T, Houtkooper RH, You X, Chen W, Zeiher AM, Potente M, Dimmeler S, Boon RA. Laminar shear stress inhibits endothelial cell metabolism via KLF2-mediated repression of PFKFB3. Arterioscler Thromb Vasc Biol. 2015; 35:137–45. [PubMed: 25359860]

32. Dodt H-U, Leischner U, Schierloh A, Jährling N, Mauch CP, Deininger K, Deussing JM, Eder M, Zieglgänsberger W, Becker K. Ultramicroscopy: three-dimensional visualization of neuronal networks in the whole mouse brain. Nature methods. 2007; 4:331. [PubMed: 17384643]

33. Eliceiri KW, Berthold MR, Goldberg IG, Ibanez L, Manjunath BS, Martone ME, Murphy RF, Peng H, Plant AL, Roysam B, Stuurman N, Swedlow JR, Tomancak P, Carpenter AE. Biological imaging software tools. Nat Methods. 2012; 9:697–710. [PubMed: 22743775]

34. Fei P, Lee J, Packard RRS, Sereti K-I, Xu H, Ma J, Ding Y, Kang H, Chen H, Sung K. Cardiac light-sheet fluorescent microscopy for multi-scale and rapid imaging of architecture and function. Scientific reports. 2016; 6:22489. [PubMed: 26935567]

35. Fei P, Nie J, Lee J, Ding Y, Li S, Yu Z, Zhang H, Hagiwara M, Yu T, Segura T. Sub-voxel light-sheet microscopy for high-resolution, high-throughput volumetric imaging of large biomedical specimens. bioRxiv. 2018:255695.

36. Forouhar AS, Liebling M, Hickerson A, Nasiraei-Moghaddam A, Tsai H-J, Hove JR, Fraser SE, Dickinson ME, Gharib M. The embryonic vertebrate heart tube is a dynamic suction pump. Science. 2006; 312:751–753. [PubMed: 16675702]

37. Frampton MW. Systemic and cardiovascular effects of airway injury and inflammation: Ultrafine particle exposure in humans. Environmental Health Perspectives. 2001; 109:529–532. [PubMed: 11544158]

38. Frangos JA, Huang TY, Clark CB. Steady shear and step changes in shear stimulate endothelium via independent mechanisms--superposition of transient and sustained nitric oxide production. Biochem Biophys Res Commun. 1996; 224:660–5. [PubMed: 8713104]

39. Fre S, Huyghe M, Mourikis P, Robine S, Louvard D, Artavanis-Tsakonas S. Notch signals control the fate of immature progenitor cells in the intestine. Nature. 2005; 435:964–8. [PubMed: 15959516]

40. Galloway JL, Wingert RA, Thisse C, Thisse B, Zon LI. Loss of gata1 but not gata2 converts erythropoiesis to myelopoiesis in zebrafish embryos. Dev Cell. 2005; 8:109–16. [PubMed: 15621534]

41. Gerhardt H, Golding M, Fruttiger M, Ruhrberg C, Lundkvist A, Abramsson A, Jeltsch M, Mitchell C, Alitalo K, Shima D. VEGF guides angiogenic sprouting utilizing endothelial tip cell filopodia. The Journal of cell biology. 2003; 161:1163–1177. [PubMed: 12810700]

42. Gorham ED, Garland CF, Garland FC. Acid haze air pollution and breast and colon cancer mortality in 20 Canadian cities. Can J Public Health. 1989; 80:96–100. [PubMed: 2720547]

43. Hellstrom M, Phng LK, Hofmann JJ, Wallgard E, Coultas L, Lindblom P, Alva J, Nilsson AK, Karlsson L, Gaiano N, Yoon K, Rossant J, Iruela-Arispe ML, Kalen M, Gerhardt H, Betsholtz C. Dll4 signalling through Notch1 regulates formation of tip cells during angiogenesis. Nature. 2007; 445:776–80. [PubMed: 17259973]

44. Herzog W, Müller K, Huisken J, Stainier DY. Genetic evidence for a noncanonical function of seryl-tRNA synthetase in vascular development. Circulation research. 2009; 104:1260–1266. [PubMed: 19423847]
45. Hogan BM, Bos FL, Bussmann J, Witte M, Chi NC, Duckers HJ, Schulte-Merker S. Ccbe1 is required for embryonic lymphangiogenesis and venous sprouting. Nature genetics. 2009; 41:396. [PubMed: 19287381]
46. Horton NG, Wang K, Kobat D, Clark CG, Wise FW, Schaffer CB, Xu C. In vivo three-photon microscopy of subcortical structures within an intact mouse brain. Nat Photon. 2013; 7:205–209.
47. Huisken J, Stainier DY. Selective plane illumination microscopy techniques in developmental biology. Development. 2009; 136:1963–1975. [PubMed: 19465594]
48. Huisken J, Swoger J, Del Bene F, Wittbrodt J, Stelzer EH. Optical sectioning deep inside live embryos by selective plane illumination microscopy. Science. 2004; 305:1007–1009. [PubMed: 15310904]
49. Hwang BF, Lee YL, Jaakkola JJ. Air Pollution and the Risk of Cardiac Defects: A Population-Based Case-Control Study. Medicine (Baltimore). 2015; 94:e1883. [PubMed: 26554783]
50. Hwang J, Michael H, Salazar A, Lassegue B, Griendling K, Navab M, Sevanian A, Hsiai TK. Pulsatile versus oscillatory shear stress regulates NADPH oxidase subunit expression: implication for native LDL oxidation. Circulation research. 2003a; 93:1225–1232. [PubMed: 14593003]
51. Hwang J, Saha A, Boo YC, Sorescu GP, McNally JS, Holland SM, Dikalov S, Giddens DP, Griendling KK, Harrison DG, Jo H. Oscillatory shear stress stimulates endothelial production of O2- from p47phox-dependent NAD(P)H oxidases, leading to monocyte adhesion. J Biol Chem. 2003b; 278:47291–8. [PubMed: 12958309]
52. Jensen J, Heller RS, Funder-Nielsen T, Pedersen EE, Lindsell C, Weinmaster G, Madsen OD, Serup P. Independent development of pancreatic alpha- and beta-cells from neurogenin3-expressing precursors: a role for the notch pathway in repression of premature differentiation. Diabetes. 2000; 49:163–76. [PubMed: 10868931]
53. Joutel A, Corpechot C, Ducros A, Vahedi K, Chabriat H, Mouton P, Alamowitch S, Domenga V, Cecillion M, Marechal E, Maciazek J, Vayssiere C, Cruaud C, Cabanis EA, Ruchoux MM, Weissenbach J, Bach JF, Bousser MG, Tournier-Lasserve E. Notch3 mutations in CADASIL, a hereditary adult-onset condition causing stroke and dementia. Nature. 1996; 383:707–10. [PubMed: 8878478]
54. Karimi Galougahi K, Ashley EA, Ali ZA. Redox regulation of vascular remodeling. Cell Mol Life Sci. 2016; 73:349–63. [PubMed: 26483132]
55. Keller PJ, Schmidt AD, Santella A, Khairy K, Bao Z, Wittbrodt J, Stelzer EH. Fast, high-contrast imaging of animal development with scanned light sheet-based structured-illumination microscopy. Nat Methods. 2010; 7:637–42. [PubMed: 20601950]
56. Keller PJ, Schmidt AD, Wittbrodt J, Stelzer EH. Reconstruction of zebrafish early embryonic development by scanned light sheet microscopy. science. 2008; 322:1065–1069. [PubMed: 18845710]
57. Keller PJ, Stelzer EHK. Quantitative in vivo imaging of entire embryos with digital scanned laser light sheet fluorescence microscopy. Curr Opin Neurobiol. 2008; 18:624–632. [PubMed: 19375303]
58. Kobat D, Horton NG, Xu C. In vivo two-photon microscopy to 1.6-mm depth in mouse cortex. J Biomed Opt. 2011; 16:106014-106014–4. [PubMed: 22029361]
59. Koh W, Sachidanandam K, Stratman AN, Sacharidou A, Mayo AM, Murphy EA, Cheresh DA, Davis GE. Formation of endothelial lumens requires a coordinated PKCepsilon-, Src-, Pak- and Raf-kinase-dependent signaling cascade downstream of Cdc42 activation. J Cell Sci. 2009; 122:1812–22. [PubMed: 19435802]
60. Krebs LT, Xue Y, Norton CR, Shutter JR, Maguire M, Sundberg JP, Gallahan D, Closson V, Kitajewski J, Callahan R, Smith GH, Stark KL, Gridley T. Notch signaling is essential for vascular morphogenesis in mice. Genes Dev. 2000; 14:1343–52. [PubMed: 10837027]
61. Kulkeaw K, Sugiyama D. Zebrafish erythropoiesis and the utility of fish as models of anemia. Stem cell research & therapy. 2012; 3:55. [PubMed: 23257067]

62. Kumar A, Wu Y, Christensen R, Chandris P, Gandler W, McCreedy E, Bokinsky A, Colón-Ramos DA, Bao Z, McAuliffe M. Dual-view plane illumination microscopy for rapid and spatially isotropic imaging. nature protocols. 2014; 9:2555. [PubMed: 25299154]
63. Lawrence S, Giles CL, Tsoi AC, Back AD. Face recognition: a convolutional neural-network approach. IEEE Trans Neural Netw. 1997; 8:98–113. [PubMed: 18255614]
64. Lee J, Cao H, Kang BJ, Jen N, Yu F, Lee C-A, Fei P, Park J, Bohlool S, Lash-Rosenberg L. Hemodynamics and ventricular function in a zebrafish model of injury and repair. Zebrafish. 2014; 11:447–454. [PubMed: 25237983]
65. Lee J, Fei P, Packard RRS, Kang H, Xu H, Baek KI, Jen N, Chen J, Yen H, Kuo C-CJ. 4-Dimensional light-sheet microscopy to elucidate shear stress modulation of cardiac trabeculation. The Journal of clinical investigation. 2016; 126:1679–1690. [PubMed: 27018592]
66. Lee J, Packard RR, Hsiai TK. Blood flow modulation of vascular dynamics. Curr Opin Lipidol. 2015; 26:376–83. [PubMed: 26218416]
67. Lenard A, Daetwyler S, Betz C, Ellertsdottir E, Belting H-G, Huisken J, Affolter M. Endothelial cell self-fusion during vascular pruning. PLoS biology. 2015; 13:e1002126. [PubMed: 25884426]
68. Li R, Beebe T, Jen N, Yu F, Takabe W, Harrison M, Cao H, Lee J, Yang H, Han P, Wang K, Shimizu H, Chen J, Lien CL, Chi NC, Hsiai TK. Shear stress-activated Wnt-angiopoietin-2 signaling recapitulates vascular repair in zebrafish embryos. Arterioscler Thromb Vasc Biol. 2014; 34:2268–75. [PubMed: 25147335]
69. Li R, Jen N, Wu L, Lee J, Fang K, Quigley K, Lee K, Wang S, Zhou B, Vergnes L, Chen YR, Li Z, Reue K, Ann DK, Hsiai TK. Disturbed Flow Induces Autophagy, but Impairs Autophagic Flux to Perturb Mitochondrial Homeostasis. Antioxid Redox Signal. 2015; 23:1207–19. [PubMed: 26120766]
70. Li R, Navab M, Pakbin P, Ning Z, Navab K, Hough G, Morgan TE, Finch CE, Araujo JA, Fogelman AM, Sioutas C, Hsiai T. Ambient ultrafine particles alter lipid metabolism and HDL anti-oxidant capacity in LDLR-null mice. J Lipid Res. 2013; 54:1608–15. [PubMed: 23564731]
71. Li R, Ning Z, Cui J, Khalsa B, Ai L, Takabe W, Beebe T, Majumdar R, Sioutas C, Hsiai T. Ultrafine particles from diesel engines induce vascular oxidative stress via JNK activation. Free Radic Biol Med. 2009; 46:775–82. [PubMed: 19154785]
72. Li R, Yang J, Saffari A, Jacobs J, Baek KI, Hough G, Larauche MH, Ma J, Jen N, Moussaoui N, Zhou B, Kang H, Reddy S, Henning SM, Campen MJ, Pisegna J, Li Z, Fogelman AM, Sioutas C, Navab M, Hsiai TK. Ambient Ultrafine Particle Ingestion Alters Gut Microbiota in Association with Increased Atherogenic Lipid Metabolites. Sci Rep. 2017; 7:42906. [PubMed: 28211537]
73. Li YS, Haga JH, Chien S. Molecular basis of the effects of shear stress on vascular endothelial cells. J Biomech. 2005; 38:1949–71. [PubMed: 16084198]
74. Liebling M, Forouhar AS, Gharib M, Fraser SE, Dickinson ME. Four-dimensional cardiac imaging in living embryos via postacquisition synchronization of nongated slice sequences. J Biomed Opt. 2005; 10:054001. [PubMed: 16292961]
75. Lobov IB, Renard RA, Papadopoulos N, Gale NW, Thurston G, Yancopoulos GD, Wiegand SJ. Delta-like ligand 4 (Dll4) is induced by VEGF as a negative regulator of angiogenic sprouting. Proc Natl Acad Sci U S A. 2007; 104:3219–24. [PubMed: 17296940]
76. Lough GC, Schauer JJ, Park JS, Shafer MM, Deminter JT, Weinstein JP. Emissions of metals associated with motor vehicle roadways. Environ Sci Technol. 2005; 39:826–36. [PubMed: 15757346]
77. MacKenzie F, Duriez P, Wong F, Noseda M, Karsan A. Notch4 inhibits endothelial apoptosis via RBP-Jkappa-dependent and -independent pathways. J Biol Chem. 2004; 279:11657–63. [PubMed: 14701863]
78. Mickoleit M, Schmid B, Weber M, Fahrbach FO, Hombach S, Reischauer S, Huisken J. High-resolution reconstruction of the beating zebrafish heart. Nature methods. 2014; 11:919. [PubMed: 25042787]
79. Minicucci MF, Azevedo PS, Paiva SA, Zornoff LA. Cardiovascular remodeling induced by passive smoking. Inflamm Allergy Drug Targets. 2009; 8:334–9. [PubMed: 20025579]
80. Nel A, Xia T, Madler L, Li N. Toxic potential of materials at the nanolevel. Science. 2006; 311:622–627. [PubMed: 16456071]

81. Nemmar A, Hoet PHM, Vanquickenborne B, Dinsdale D, Thomeer M, Hoylaerts MF, Vanbilloen H, Mortelmans L, Nemery B. Passage of inhaled particles into the blood circulation in humans. Circulation. 2002; 105:411–414. [PubMed: 11815420]
82. Nguyen D-HT, Stapleton SC, Yang MT, Cha SS, Choi CK, Galie PA, Chen CS. Biomimetic model to reconstitute angiogenic sprouting morphogenesis in vitro. Proceedings of the National Academy of Sciences. 2013; 110:6712–6717.
83. Ntziachristos V, Ripoll J, Wang LV, Weissleder R. Looking and listening to light: the evolution of whole-body photonic imaging. Nat Biotechnol. 2005; 23:313–320. [PubMed: 15765087]
84. Opitz R, Maquet E, Huisken J, Antonica F, Trubiroha A, Pottier G, Janssens V, Costagliola S. Transgenic zebrafish illuminate the dynamics of thyroid morphogenesis and its relationship to cardiovascular development. Developmental biology. 2012; 372:203–216. [PubMed: 23022354]
85. Packard RRS, Baek KI, Beebe T, Jen N, Ding Y, Shi F, Fei P, Kang BJ, Chen P-H, Gau J. Automated Segmentation of Light-Sheet Fluorescent Imaging to Characterize Experimental Doxorubicin-Induced Cardiac Injury and Repair. Sci Rep. 2017; 7:8603. [PubMed: 28819303]
86. Pellegrinet L, Rodilla V, Liu Z, Chen S, Koch U, Espinosa L, Kaestner KH, Kopan R, Lewis J, Radtke F. Dll1- and dll4-mediated notch signaling are required for homeostasis of intestinal stem cells. Gastroenterology. 2011; 140:1230–1240. e1–7. [PubMed: 21238454]
87. Peng H, Ruan Z, Long F, Simpson JH, Myers EW. V3D enables real-time 3D visualization and quantitative analysis of large-scale biological image data sets. Nat Biotechnol. 2010; 28:348–53. [PubMed: 20231818]
88. Peng H, Tang J, Xiao H, Bria A, Zhou J, Butler V, Zhou Z, Gonzalez-Bellido PT, Oh SW, Chen J, Mitra A, Tsien RW, Zeng H, Ascoli GA, Iannello G, Hawrylycz M, Myers E, Long F. Virtual finger boosts three-dimensional imaging and microsurgery as well as terabyte volume image visualization and analysis. Nat Commun. 2014; 5:4342. [PubMed: 25014658]
89. Pope CA 3rd, Burnett RT, Thurston GD, Thun MJ, Calle EE, Krewski D, Godleski JJ. Cardiovascular mortality and long-term exposure to particulate air pollution: epidemiological evidence of general pathophysiological pathways of disease. Circulation. 2004; 109:71–7. [PubMed: 14676145]
90. Power RM, Huisken J. A guide to light-sheet fluorescence microscopy for multiscale imaging. Nature methods. 2017; 14:360. [PubMed: 28362435]
91. Quillard T, Coupel S, Coulon F, Fitau J, Chatelais M, Cuturi MC, Chiffoleau E, Charreau B. Impaired Notch4 activity elicits endothelial cell activation and apoptosis: implication for transplant arteriosclerosis. Arterioscler Thromb Vasc Biol. 2008; 28:2258–65. [PubMed: 18802018]
92. Rask-Madsen C, King GL. Differential regulation of VEGF signaling by PKC-alpha and PKC-epsilon in endothelial cells. Arterioscler Thromb Vasc Biol. 2008; 28:919–24. [PubMed: 18323518]
93. Ritz B, Yu F, Fruin S, Chapa G, Shaw GM, Harris JA. Ambient air pollution and risk of birth defects in Southern California. Am J Epidemiol. 2002; 155:17–25. [PubMed: 11772780]
94. Rodosthenous RS, Coull BA, Lu Q, Vokonas PS, Schwartz JD, Baccarelli AA. Ambient particulate matter and microRNAs in extracellular vesicles: a pilot study of older individuals. Part Fibre Toxicol. 2016; 13:13. [PubMed: 26956024]
95. Roman BL, Pekkan K. Mechanotransduction in embryonic vascular development. Biomech Model Mechanobiol. 2012; 11:1149–68. [PubMed: 22744845]
96. Rostama B, Peterson SM, Vary CP, Liaw L. Notch signal integration in the vasculature during remodeling. Vascul Pharmacol. 2014; 63:97–104. [PubMed: 25464152]
97. Santi PA. Light sheet fluorescence microscopy: a review. J Histochem Cytochem. 2011; 59:129–138. [PubMed: 21339178]
98. Sardar SB, Fine PM, Mayo PR, Sioutas C. Size-fractionated measurements of ambient ultrafine particle chemical composition in Los Angeles using the NanoMOUDI. Environ Sci Technol. 2005; 39:932–44. [PubMed: 15773464]
99. Schmid B, Shah G, Scherf N, Weber M, Thierbach K, Campos CP, Roeder I, Aanstad P, Huisken J. High-speed panoramic light-sheet microscopy reveals global endodermal cell dynamics. Nat Commun. 2013; 4:2207. [PubMed: 23884240]

100. Schulz H, Harder V, Ibald-Mulli A, Khandoga A, Koenig W, Krombach F, Radykewicz R, Stampfl A, Thorand B, Peters A. Cardiovascular effects of fine and ultrafine particles. J Aerosol Med. 2005; 18:1–22. [PubMed: 15741770]
101. Shelhamer E, Long J, Darrell T. Fully Convolutional Networks for Semantic Segmentation. IEEE Trans Pattern Anal Mach Intell. 2017; 39:640–651. [PubMed: 27244717]
102. Sideris E, Griffin DR, Ding Y, Li S, Weaver WM, Di Carlo D, Hsiai T, Segura T. Particle hydrogels based on hyaluronic acid building blocks. ACS Biomater Sci Engin. 2016; 2:2034–2041.
103. Simmons RD, Kumar S, Jo H. The role of endothelial mechanosensitive genes in atherosclerosis and omics approaches. Arch Biochem Biophys. 2016; 591:111–31. [PubMed: 26686737]
104. Stanger BZ, Datar R, Murtaugh LC, Melton DA. Direct regulation of intestinal fate by Notch. Proc Natl Acad Sci U S A. 2005; 102:12443–8. [PubMed: 16107537]
105. Suarez J, Rubio R. Regulation of glycolytic flux by coronary flow in guinea pig heart. Role of vascular endothelial cell glycocalyx. Am J Physiol. 1991; 261:H1994–2000. [PubMed: 1750547]
106. Sun P, Zhang Y, Yu F, Parks E, Lyman A, Wu Q, Ai L, Hu C-H, Zhou Q, Shung K. Micro-electrocardiograms to study post-ventricular amputation of zebrafish heart. Ann Biomed Eng. 2009; 37:890–901. [PubMed: 19280341]
107. Sung K, Ding Y, Ma J, Chen H, Huang V, Cheng M, Yang CF, Kim JT, Eguchi D, Carlo DD, Hsiai TK, Nakano A, Kulkarni RP. Simplified three-dimensional tissue clearing and incorporation of colorimetric phenotyping. Sci Rep. 2016; 6:30736. [PubMed: 27498769]
108. Surapisitchat J, Hoefen RJ, Pi X, Yoshizumi M, Yan C, Berk BC. Fluid shear stress inhibits TNF-alpha activation of JNK but not ERK1/2 or p38 in human umbilical vein endothelial cells: Inhibitory crosstalk among MAPK family members. Proc Natl Acad Sci U S A. 2001; 98:6476–81. [PubMed: 11353829]
109. Tomer R, Khairy K, Amat F, Keller PJ. Quantitative high-speed imaging of entire developing embryos with simultaneous multiview light-sheet microscopy. Nat Methods. 2012; 9:755–63. [PubMed: 22660741]
110. Tomer R, Lovett-Barron M, Kauvar I, Andalman A, Burns VM, Sankaran S, Grosenick L, Broxton M, Yang S, Deisseroth K. SPED light sheet microscopy: Fast mapping of biological system structure and function. Cell. 2015; 163:1796–1806. [PubMed: 26687363]
111. Truong TV, Supatto W, Koos DS, Choi JM, Fraser SE. Deep and fast live imaging with two-photon scanned light-sheet microscopy. Nat Methods. 2011; 8:757–60. [PubMed: 21765409]
112. Tzahor E, Poss KD. Cardiac regeneration strategies: Staying young at heart. Science. 2017; 356:1035–1039. [PubMed: 28596337]
113. Vermot J, Forouhar AS, Liebling M, Wu D, Plummer D, Gharib M, Fraser SE. Reversing blood flows act through klf2a to ensure normal valvulogenesis in the developing heart. PLoS biology. 2009; 7:e1000246. [PubMed: 19924233]
114. Vladimirov N, Mu Y, Kawashima T, Bennett DV, Yang CT, Looger LL, Keller PJ, Freeman J, Ahrens MB. Light-sheet functional imaging in fictively behaving zebrafish. Nat Methods. 2014; 11:883–4. [PubMed: 25068735]
115. Volkova M, Russell R 3rd. Anthracycline cardiotoxicity: prevalence, pathogenesis and treatment. Curr Cardiol Rev. 2011; 7:214–20. [PubMed: 22758622]
116. Walshe TE, Connell P, Cryan L, Ferguson G, Gardiner T, Morrow D, Redmond EM, O'Brien C, Cahill PA. Microvascular retinal endothelial and pericyte cell apoptosis in vitro: role of hedgehog and Notch signaling. Invest Ophthalmol Vis Sci. 2011; 52:4472–83. [PubMed: 21498615]
117. Weber M, Scherf N, Meyer AM, Panakova D, Kohl P, Huisken J. Cell-accurate optical mapping across the entire developing heart. Elife. 2017:6.
118. Wu D, Huang RT, Hamanaka RB, Krause M, Oh MJ, Kuo CH, Nigdelioglu R, Meliton AY, Witt L, Dai G, Civelek M, Prabhakar NR, Fang Y, Mutlu GM. HIF-1alpha is required for disturbed flow-induced metabolic reprogramming in human and porcine vascular endothelium. Elife. 2017:6.
119. Wu L, Li H, Jia CY, Cheng W, Yu M, Peng M, Zhu Y, Zhao Q, Dong YW, Shao K, Wu A, Wu XZ. MicroRNA-223 regulates FOXO1 expression and cell proliferation. FEBS Lett. 2012; 586:1038–43. [PubMed: 22569260]

120. Wu Y, Ghitani A, Christensen R, Santella A, Du Z, Rondeau G, Bao Z, Colon-Ramos D, Shroff H. Inverted selective plane illumination microscopy (iSPIM) enables coupled cell identity lineaging and neurodevelopmental imaging in Caenorhabditis elegans. Proc Natl Acad Sci U S A. 2011; 108:17708–13. [PubMed: 22006307]

121. Wu Y, Wawrzusin P, Senseney J, Fischer RS, Christensen R, Santella A, York AG, Winter PW, Waterman CM, Bao Z. Spatially isotropic four-dimensional imaging with dual-view plane illumination microscopy. Nature biotechnology. 2013; 31:1032.

122. Yang L, Hou XY, Wei Y, Thai P, Chai F. Biomarkers of the health outcomes associated with ambient particulate matter exposure. Sci Total Environ. 2017; 579:1446–1459. [PubMed: 27908628]

123. Yu B, Zhou S, Wang Y, Qian T, Ding G, Ding F, Gu X. miR-221 and miR-222 promote Schwann cell proliferation and migration by targeting LASS2 after sciatic nerve injury. J Cell Sci. 2012; 125:2675–83. [PubMed: 22393241]

124. Yuste R. Fluorescence microscopy today. Nat Methods. 2005; 2:902–4. [PubMed: 16299474]

125. Zhang Y, Schauer JJ, Shafer MM, Hannigan MP, Dutton SJ. Source apportionment of in vitro reactive oxygen species bioassay activity from atmospheric particulate matter. Environ Sci Technol. 2008; 42:7502–9. [PubMed: 18939593]

126. Zheng S, Jayasumana S, Romera-Paredes B, Vineet V, Su Z, Du D, Huang C, Torr PH. Book Conditional random fields as recurrent neural networks. City: 2015. Conditional random fields as recurrent neural networks; 1529–1537.

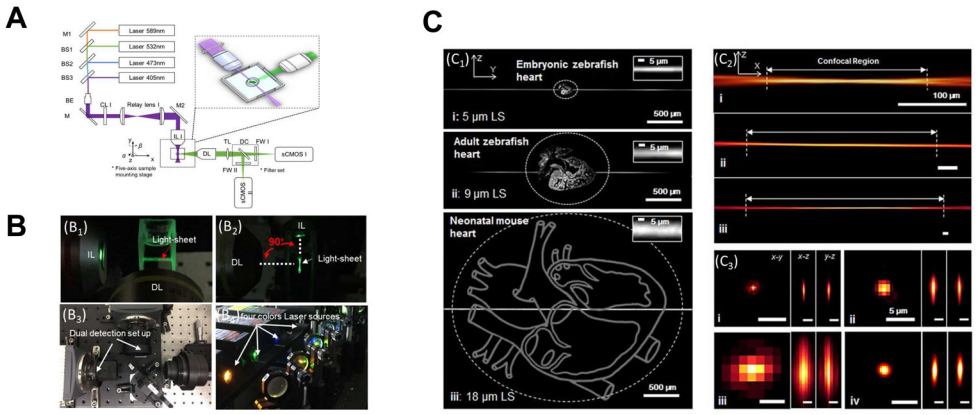

Figure 1. Schematic diagram and performance of the fluorescent light-sheet microscope

(**A**) Four collimated laser sources were focused through a cylindrical lens and transmitted by illumination lens (IL) to generate a light-sheet sectioning the sample. The objective lens (DL) was positioned orthogonally to the illumination path for fluorescence detection. In addition, the dual-channel detection was achieved using a dichroic mirror and filter sets at the detection arm. The focus of detection needs to be exactly conjugated to the illuminated plane. **(B_1)** The formation of the light-sheet from the illumination objectives and detected by detection objectives. **(B_2)** Top view of the light-sheet demonstrated orthogonal relation between IL and DL. **(B_3)** Four laser wavelengths offer flexibility for different fluorophores. M: mirror; DC: dichroic mirror; BE: beam expander; CL: cylindrical lens; SL: scan lens; TL: tube lens; FW: filter wheel; IL: illumination lens; DL: detection lens. **(B_4)** The two orthogonal cameras allowed for the capability of simultaneous dual-channel detection. **(C_1)** The axial confinement of the light-sheet was used for sectioning the (i) embryonic zebrafish, (ii) adult zebrafish, and (iii) neonatal mouse hearts. LS: light-sheet. **(C_2)** The changes in confocal region corresponded to the area available for light-sheet sectioning. The double-headed arrow line indicates the confocal region, in which the light-sheet is considered to be uniform. The scale bars are 100 μm in length for the sub-images in (i), (ii) and (iii). **(C_3)** Imaging a 400 nm fluorescent bead (sub-resolution point source) was compared with the (i) 5 μm LS detected by the 20x/0.5 DL, (ii) 9 μm LS by 10x/0.3 DL, (iii) 18 μm LS by 4x/0.13 DL and (iv) 18 μm LS by 4x/0.13 DL, with resolution enhancement applied.

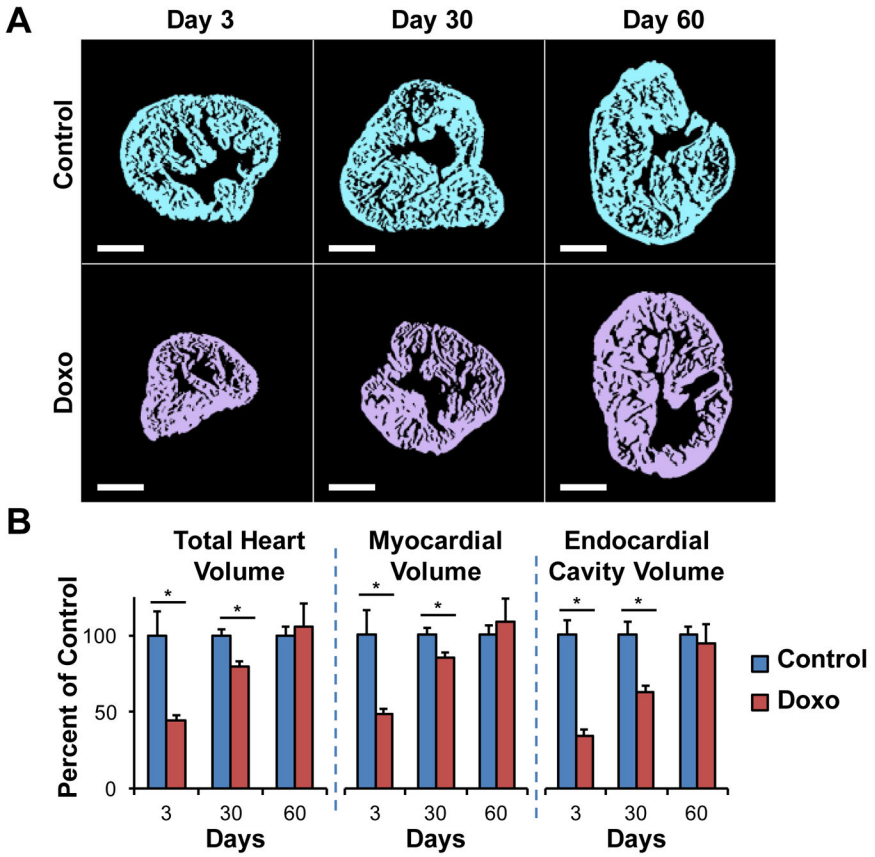

Figure 2. Light-sheet imaging to analyze doxorubicin-induced cardiac injury and regeneration

Adult zebrafish hearts were isolated at days 3, 30, 60 following intraperitoneal treatment with doxorubicin or control vehicle. **(A)** Control zebrafish hearts exhibited a preserved architecture during the study period. Treatment of doxorubicin induced a dramatic cardiac remodeling leading to an acute reduction in size at day 3, followed by a gradual increase at day 30, and normalization at day 60. **(B)** Total heart, myocardial, and endocardial volumes were quantitatively compared to control values demonstrating the regeneration process following doxorubicin-induced injury (** $P < 0.01$ vs control). Doxo: doxorubicin. Scale bar: 200 μm.

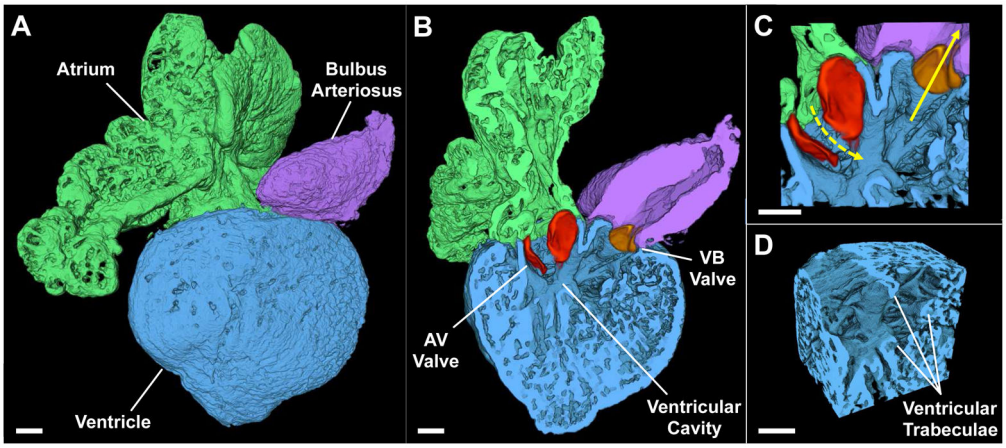

Figure 3. 3D rendering of the adult zebrafish heart

(A) 3-D rendering combined with automated segmentation method provided anatomic structures of the intact atrium, ventricle, and bulbous arteriosus in adult zebrafish heart. **(B)** Precise assessment of zebrafish heart with automated segmentation established a cross-section through the atrium, ventricle, and bulbous arteriosus and demonstrated 2 leaflets of the AV valve (red) and of the VB valve (orange). **(C)** Ventricular inflow (dotted yellow line) and outflow path (solid yellow line) were estimated with computation of the angle between the atrioventricular (AV) valves and ventricular-bulbar (VB) valves. Scale bar: 100 μm.

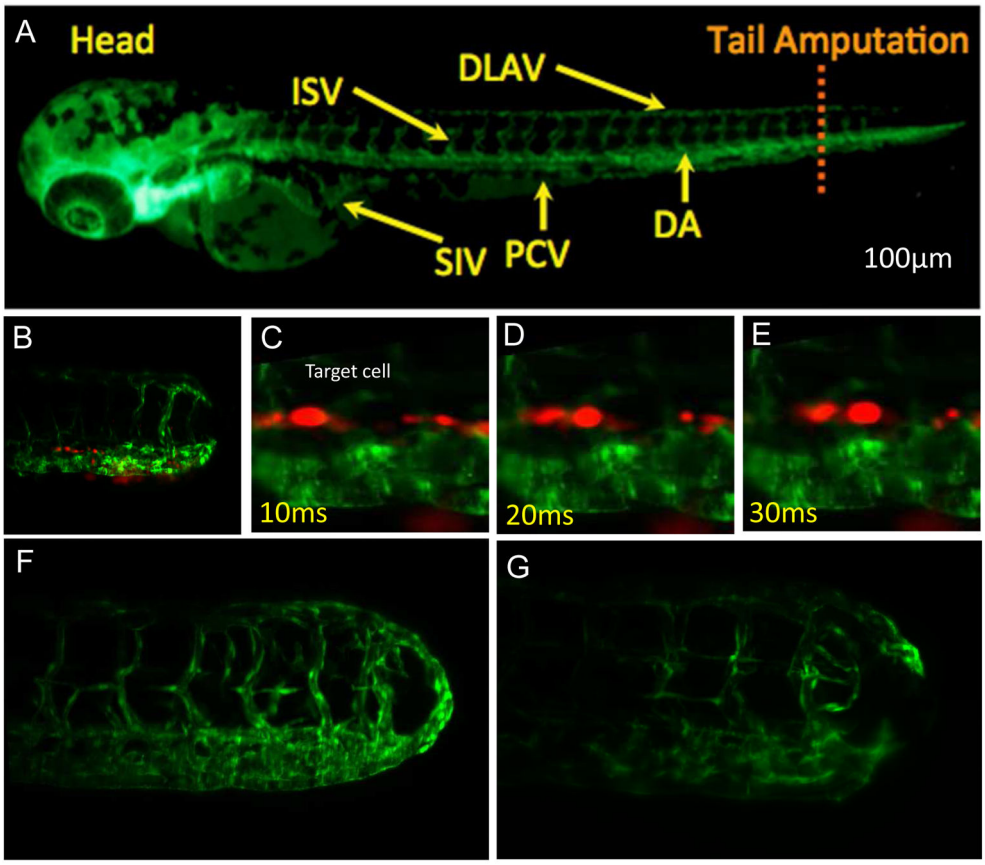

Figure 4. Light-sheet imaging of vascular regeneration and circulating erythrocytes in response to tail amputation

(A) An inverted fluorescence image demonstrated the vasculature (green) and amputation region (dashed line) of a transgenic *Tg(flk1:GFP; Gata1:Ds-Red)* zebrafish embryo at 3 dpf. ISV: intersegmental vessel; DLAV: dorsal longitudinal anastomotic vessel; SIV: subintestinal vessel; PCV: posterior cardinal vein; DA: dorsal aorta. **(B)** LSFM imaging of the erythrocytes (red) adjacent to the site of amputation and regeneration. The dashed white box indicated locations of higher power images in the subsequent panels **(C–E)**. An individual erythrocyte (red) in relation to the vascular endothelial layer (green) was tracked under LSFM at 100 fps. The travel distance and net velocity of each erythrocyte could be measured from the corresponding location difference among images **(C)**, **(D)** and **(E).** The complete **(F)** and incomplete **(G)** vascular regeneration between DLAV and DA were revealed in separate zebrafish embryos at 3 days after tail amputation. Scale bars: 25 μm.

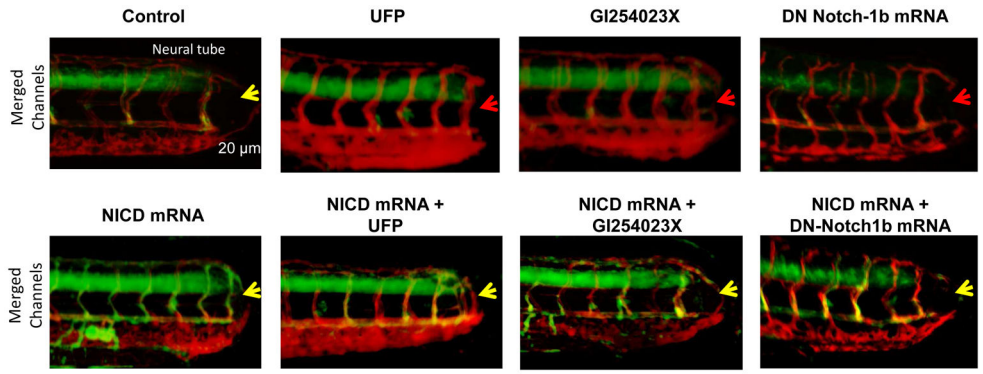

Figure 5. Ambient UFP exposure impaired Notch-mediated vascular regeneration

Transgenic *Tg(tp1:GFP; flk1:mCherry)* zebrafish embryos revealed Notch activity in the vasculature, as indicated by the overlapped yellow color, corroborating the role of endothelial Notch activity in the site of vascular repair. The control group developed vascular regeneration at 3 days post tail amputation (dpa). UFP or ADAM 10 inhibitor (GI254023X) treatment attenuated endothelial Notch activity in the site of injury and impaired vascular regeneration. Injection of dominant negative (DN)-*Notch1b* mRNA further attenuated Notch signaling-mediated vascular regeneration. As a corollary, *NICD* mRNA injection upregulated Notch activity and rescued UFP-, ADAM10 inhibitor- or DN-*Notch1b* mRNA-impaired vascular regeneration.

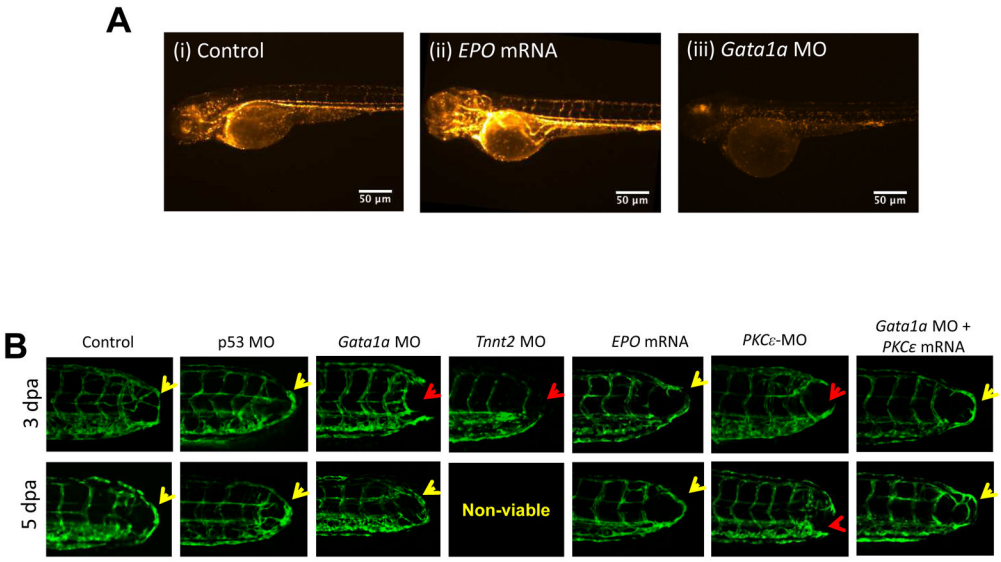

Figure 6. Shear stress is implicated in *PKCε*-dependent vascular repair

(A) Blood viscosity of the embryonic zebrafish was genetically manipulated to alter the level of endothelial wall shear stress. Compared to control embryos, micro-injection of *Gata1a* MO reduced the level of erythropoiesis and consequent wall shear stress, whereas erythropoietin (*EPO*) mRNA resulted in the opposite effect. **(B)** The control and *p53* MO-injected fish developed vascular repair at 3 dpa (yellow arrows). Reduction of viscosity-mediated shear stress with *Gata1a* MO delayed vascular repair from 3 dpa to 5 dpa. The presence of *Tnnt2* MO to arrest myocardial contractility led impaired vascular repair at 3 dpa, while embryos failed to thrive at 5 dpa (red arrow). On the other hand, increased level of erythropoiesis with *EPO* mRNA promoted vascular regeneration. Silencing *PKCε* with MO attenuated vascular repair at both 3 and 5 dpa, whereas upregulation of *PKCε* mRNA restored vascular impairment in *Gata1a* MO injected embryos.

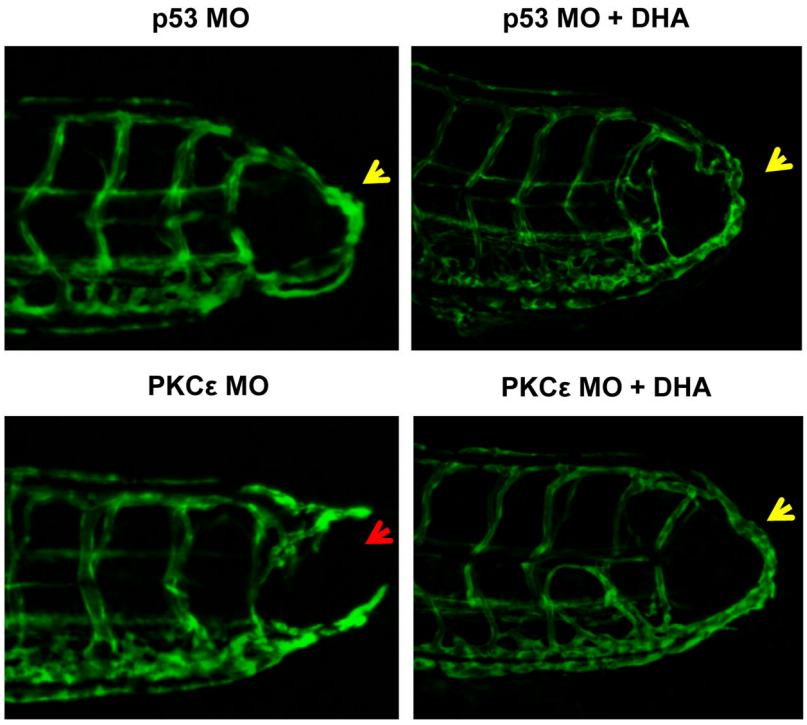

Figure 7. Glycolytic metabolite, dihydroxyacetone (DHA) promoted vascular regeneration

Transgenic *Tg(flk1:GFP)* embryos injected with control *P53* MO or *PKCε* MO were treated with or without DHA at 1mg/mL for 3 days after initial vascular injury. Micro-injection of *PKCε* MO resulted in impaired vascular regeneration (red arrow), whereas DHA treatment reversed the effect of *PKCε* MO and promoted vascular regeneration (yellow arrows).

Table 1

Comparative advantages and disadvantages among different imaging modalities

Method	Lateral-Axial Resolution (nm)	Penetration (μm)	Image acquisition time	Advantage	Disadvantage
LSFM	200–500	>1000	ms-s	Low phototoxicity	Big data
CFM	200–400	150	s-mins	Optical sectioning	Scanning
WFM	250	---	ms-mins	Low cost, user-friendly design	Low contrast
SD-CFM	200–400	150	s-mins	Rapid Image acquisition	Fixed pinhole
MPM	300–500	1000	ms-mins	Penetration depth, intrinsic confocality	Requires high power pulsed laser
STED	80–400	50	s-mins	High resolution at confocal speed	Significant photobleaching
PALM/STORM	50–100	0.1	mins-hr	Extremely high resolution	Slow image acquisition

LSFM: light-sheet fluorescence microscopy; CFM: confocal microscopy; WFM: wide-field microscopy; SD-CFM: spinning disk confocal microscopy; MPM: multi-photon microscopy; STED: stimulated emission depletion; PALM: photo-activated localization microscopy; STORM: stochastic optical reconstruction microscopy. Adapted from Ding Y et al., Curr. Cardiol. Rep., 2018.